



Comparative Energy and Emission Analysis of Oxy-Combustion and Conventional Air Combustion

Ibrahim Ozsari¹ · Yasin Ust¹ · Hasan Kayhan Kayadelen²

Received: 3 June 2020 / Accepted: 11 November 2020 / Published online: 3 January 2021
© King Fahd University of Petroleum & Minerals 2021

Abstract

Carbon capture and storage and oxy-fuel combustion have recently become more significant due to global warming as well as green energy solutions. Oxy-combustion power plants fueled with natural gas are compatible with today's clean energy policies. In this study, effects of oxygen content of reactant mixtures used in oxy-combustion on thermodynamic properties, adiabatic flame temperatures, combustion products and pollutant emissions are analyzed using a novel multi-feature equilibrium combustion model. Using natural gas from most important origins (Russia, USA, Iran, Australia) as fuel, results obtained from oxy-fuel combustion for three different O₂ fractions are compared with the results of conventional air–fuel combustion for varying equivalence ratio, inlet temperature and pressure. The accuracy of the results is confirmed by two different popular combustion softwares. According to the results, oxy-fuel combustion of same oxygen content with air causes 24% less entropy production but 40 times less NO_x emissions which is an indicator of significant decrease in carbon capture and storage costs. Comparison of natural gas of different origins shows that Russian natural gas is more advantageous in terms of NO_x emissions where Australian natural gas is more advantageous in terms of entropy production.

Keywords Chemical equilibrium · Emissions · Flue gas analysis · Natural gas · Oxy-combustion · Thermodynamic properties

List of Symbols

<i>a</i>	Mole number of reactant O ₂
<i>b</i>	Mole number of reactant CO ₂
<i>c</i>	Mole number of reactant N ₂
<i>C</i>	Specific heat (kJ/kg K)
CC	Combustion chamber
<i>E</i>	Energy
FA	Fuel/air ratio
<i>h</i>	Specific enthalpy (kJ/kg)
<i>K</i>	Equilibrium constant
MW	Molecular weight
<i>N</i>	Total number of moles of species
NG	Natural gas
<i>s</i>	Specific entropy (kJ/kg K)
<i>T</i>	Temperature (K)

<i>V</i>	Volume
<i>X</i>	Total number of carbon atoms
<i>Y</i>	Total number of hydrogen atoms
<i>Z</i>	Total number of oxygen atoms
<i>Q</i>	Total number of nitrogen atoms

Greek Symbols

α	Mole fraction
ϵ	Molar air–fuel ratio
Φ	Equivalence ratio
χ	Number of moles of exhaust species

Subscripts

<i>a</i>	Air
<i>ady</i>	Adiabatic
<i>f</i>	Fuel
<i>fu</i>	Fluid or oxidant
<i>in</i>	Inlet
<i>k</i>	Exhaust species
<i>p</i>	Pressure
<i>r</i>	Reactants
<i>s</i>	Stoichiometric
<i>wf</i>	Working fluid
<i>x</i>	Number of carbon atoms
<i>y</i>	Number of hydrogen atoms

✉ Ibrahim Ozsari
ozsari@yildiz.edu.tr; ibrahimozsari@gmail.com

¹ Department of Naval Architecture and Marine Engineering, Yildiz Technical University, 34349 Besiktas, Istanbul, Turkey

² Department of Marine Engineering Operations, Yildiz Technical University, 34349 Besiktas, Istanbul, Turkey



- z Number of oxygen atoms
 q Number of nitrogen atoms

1 Introduction

Energy demand in recent years is increasing with a growing rate. Increasing awareness of global warming phenomenon led researches on green energy production systems. In the meantime, increase in penalties for excessive pollutant emissions raises zero emission power plant concepts. Burning of fossil fuels causes very harmful emissions such as NO_x and increases greenhouse gas emissions in the atmosphere. Among these greenhouse gases, carbon dioxide undoubtedly has the greatest importance in terms of global warming. For many years studies have been carried out to reduce the amount of carbon dioxide emissions of power production plants.

In order to be effective in the competition against global warming and climate change, intensive work is being carried out on carbon dioxide capture, transport, and storage (CCS). Three basic technologies for CCS are post-combustion, pre-combustion and oxy-combustion systems [1], namely, used to keep carbon dioxide concentrations resulting from the combustion of fuels within specified limits. The operating principles of these systems are shown in Fig. 1. Oxy-fuel combustion technology utilizes a thermodynamic cycle in which the fuel is burned in a combustion chamber with an oxidant stream of pure O_2 and flue gas with high quantity CO_2 and almost zero N_2 is aimed in order to capture CO_2 more effectively. This is more difficult in air power cycles with traditional air combustors because N_2 forms a large proportion of the air and it reacts with fuel in the combustion process which causes NO_x emissions. With oxy-fuel combustion, carbon dioxide can be easily captured and stored which consequently minimizes energy and investment costs significantly.

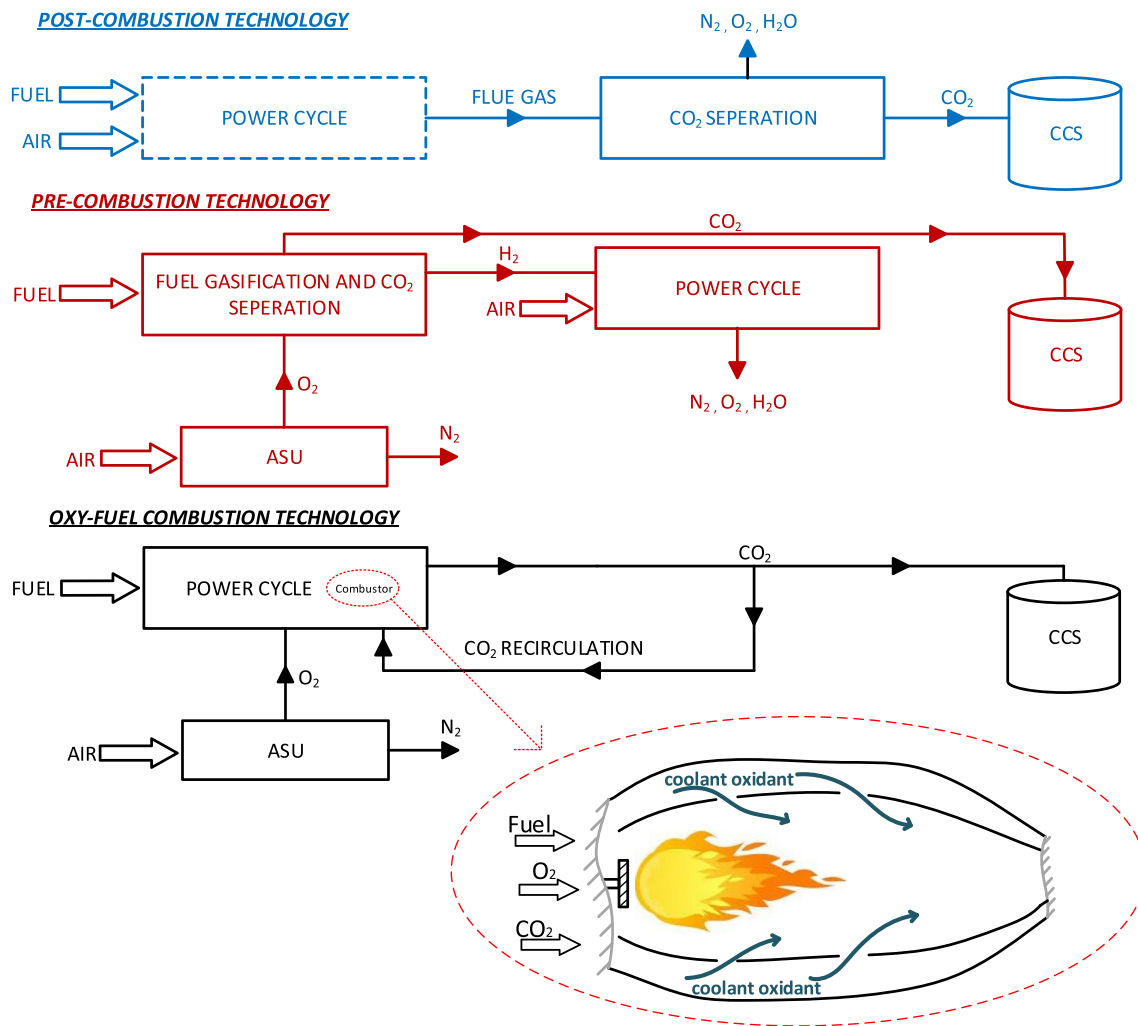


Fig. 1 Carbon capture and storage technologies and oxy-fuel combustion in detail



In oxy-fuel combustion power systems, very high combustion temperatures occur due to the absence of N_2 among the reactants. In today's technology, the combustion temperatures in oxy-combustion power cycles can be reduced by two different technological solutions within material limits: one, as in SCOC-CC, MATIANT, and NET Power cycles, dilution of cycle working fluid with carbon dioxide [2–10] and the other, as in Graz and CES cycles, dilution of cycle working fluid with steam [11]. Comparative thermodynamic, environmental and economic investigations of these oxy-combustion cycles have been conducted in previous studies [12–14].

In the focus of current studies, the use of CO_2 instead of air in conventional power cycles has been a trend. There are many studies on oxy-combustion which comparatively investigate oxy-fuel power cycles by taking certain criteria such as power, efficiency, economy, and pollutant emissions, into consideration [15–19]. These studies show that some oxy-combustion cycles are better in terms of economy while some others in terms of pollutant emissions [20]. Some studies also focus on system components such as air separation unit (ASU), combustion chamber and carbon capture (CCS) unit [21–29]. There are also many modifications which have been applied to increase oxy-combustion cycle efficiencies [30–38].

Various studies on supercritical carbon dioxide fluidized closed cycles including thermodynamic cycle analysis in oxy-combustion power plants conclude that oxy-fuel systems using carbon dioxide as working fluid at supercritical phase is more effective in terms of thermal efficiency [30, 39–43].

Studies on characteristics of oxy-combustion at different conditions with various parameters have also been carried out [44–48]. Although flame temperature, combustion products and thermodynamic properties of the combustion products are of important concerns for optimization of thermodynamic cycles [49–54] there are no studies available which investigate these fundamental characteristics of oxy-fuel combustion systems.

In this study, in order to obtain these fundamental characteristics a detailed equilibrium combustion model is needed as it has been used in the above studies. For this aim a detailed and validated equilibrium combustion model which has been established by [55] has been modified in order to obtain flame temperature, combustion products and thermodynamic properties of the combustion products such as entropy, enthalpy and specific heat. Effects of thermal dissociations have been taken into account for better accuracy. Assessment of oxy-combustion at different oxygen ratios in comparison with conventional combustion is demonstrated and discussed for natural gas of four different origins (Russia, USA, Iran, and Australia). One other novelty of this study is the comparison of these gases in oxy-combustion

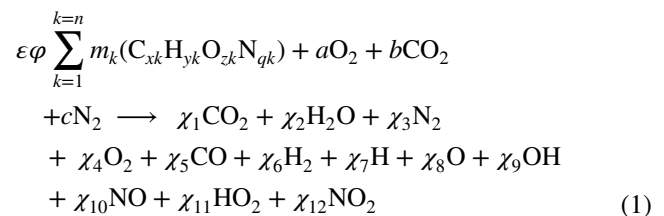
which is absent in the available literature. In addition, environmental effects of these gases and three different oxygen ratios are compared. Oxy-combustion and conventional air combustion results have been shown. Obtained results are validated by two popular combustion softwares: NASA CEA and GASEQ.

2 Materials and Methods

In order to perform a thermodynamic analysis of oxy-combustion power plants, the combustion process in the combustion chamber should be examined in detail as temperature, product concentration, specific heat, enthalpy, entropy values are important data for analysis. Besides, combustion and fuels are very important for emissions. In order to investigate the thermodynamic properties, combustion products and adiabatic flame temperature, a novel equilibrium combustion model is modified for oxy-fuel combustion regarding 12 combustion products. Analysis conducted using the equilibrium combustion model, considering all gases as ideal, and the enthalpy and specific heat of the gases as a function of temperature, and the equivalence ratios (ϕ) in the oxy-combustion are about 0.3–1.5 range. Conventional combustion has been analyzed assuming that air is composed of 21% O_2 and 79% N_2 and in dry condition. Calculations to be made in oxy-combustion are considered to be in various O_2 fractions and CO_2 is used for dilution. The very small amounts of N_2 which would leak into the system from ASU are neglected.

2.1 Mathematical Modeling for Equilibrium Combustion Products

The global chemical combustion mechanism used in the model is given below:



Here, atom numbers in fuel chemical formula are denoted as x (carbon), y (hydrogen), z (oxygen), and q (nitrogen), the molar reaction coefficients of products are denoted as χ_1 to χ_{12} , the equivalence ratio is denoted as ϕ , molar stoichiometric fuel–air ratio is denoted as ε , used to convert the amount of fuel and air in mass basis to molar basis, and the mixture reaction coefficients are denoted as a (O_2), b (CO_2) and c (N_2). In Eq. (1), a represents the oxygen supplied by

ASU, b represents recirculating CO_2 and c represents N_2 leaks from ASU.

On the other hand, in conventional combustion with air a and c are 0.21 and 0.79, respectively.

The stoichiometric equivalence ratio is defined as the ratio of fuel–air ratio (FA) over stoichiometric fuel–air ratio (FA_s):

$$\phi = \frac{\text{FA}}{\text{FA}_s} \quad (2)$$

The equivalence ratio, ϕ , of the multiple-component fuel mixture is as follows:

$$\phi = \sum_{k=1}^{k=n} \left(\frac{\text{FA}}{\text{FA}_s} \right)_k \quad (3)$$

Natural gas is the most common fuel utilized in oxy-combustion power plants. Natural gas is composed of 5–6 components, found in majority. In this study, natural gas contents from most important origins (Russia, USA, Iran, Australia) are considered [56, 57]. In oxy-combustion and conventional air combustion comparative analysis, NG01 is used. Additionally, the other 4 natural gases are examined.

C, H, O, and N atoms in fuel composition are calculated as follows:

$$X = f_1x_1 + f_2x_2 + f_3x_3 + \dots + f_nx_n \quad (4)$$

$$Y = f_1y_1 + f_2y_2 + f_3y_3 + \dots + f_ny_n \quad (5)$$

$$Z = f_1z_1 + f_2z_2 + f_3z_3 + \dots + f_nz_n \quad (6)$$

$$Q = f_1q_1 + f_2q_2 + f_3q_3 + \dots + f_nq_n \quad (7)$$

$$\varepsilon = \frac{4a}{4X + Y - 2Z} \quad (8)$$

$$R_k = \varepsilon \phi f_k \quad (9)$$

$$\text{FA}_k = \frac{R_k \text{MW}_k}{\text{MW}_{\text{fu}}} \quad (10)$$

where the oxidant molecular weight is MW_{fu} used in combustion reaction. We obtain stoichiometric fuel–air ratio is rewritten follows:

$$\text{FA}_s = \varepsilon \left[\frac{12.01x + 1.008y + 16z + 14.01q}{\text{MW}_{\text{fu}}} \right] \quad (11)$$

To calculate the products mole numbers, 12 unknowns, given in Eq. (1), a system of 12 equations can be expressed using the combustion reaction at chemical equilibrium using the following product species [58]:

$$1/2\text{H}_2 \rightleftharpoons \text{H} \quad K_1 = \alpha_1 \sqrt{p} / \sqrt{\alpha_6} \quad c_1 = K_1 / \sqrt{p} \quad \alpha_7 = c_1 / \sqrt{\alpha_6} \quad (12a)$$

$$1/2\text{O}_2 \rightleftharpoons \text{O} \quad K_2 = \alpha_8 \sqrt{p} / \sqrt{\alpha_4} \quad c_2 = K_2 / \sqrt{p} \quad \alpha_8 = c_2 / \sqrt{\alpha_4} \quad (12b)$$

$$1/2\text{H}_2 + 1/2\text{O}_2 \rightleftharpoons \text{OH} \quad K_3 = \alpha_9 / \sqrt{\alpha_4} \sqrt{\alpha_6} \\ c_3 = K_3 \quad \alpha_9 = c_3 / \sqrt{\alpha_4} \sqrt{\alpha_6} \quad (12c)$$

$$1/2\text{O}_2 + 1/2\text{N}_2 \rightleftharpoons \text{NO} \quad K_4 = \alpha_{10} / \sqrt{\alpha_4} \sqrt{\alpha_3} \\ c_4 = K_4 \quad \alpha_{10} = c_4 / \sqrt{\alpha_4} \sqrt{\alpha_3} \quad (12d)$$

$$\text{H}_2 + 1/2\text{O}_2 \rightleftharpoons \text{H}_2\text{O} \quad K_5 = \alpha_2 / \alpha_6 \sqrt{\alpha_4} \sqrt{p} \\ c_5 = K_5 \sqrt{p} \quad \alpha_2 = c_5 \alpha_6 \sqrt{\alpha_4} \quad (12e)$$

$$\text{CO} + 1/2\text{O}_2 \rightleftharpoons \text{CO}_2 \quad K_6 = \alpha_1 / \alpha_5 \sqrt{\alpha_4} \sqrt{p} \\ c_6 = K_6 \sqrt{p} \quad \alpha_1 = c_6 \alpha_5 \sqrt{\alpha_4} \quad (12f)$$

$$\text{O}_2 + 1/2\text{H}_2 \rightleftharpoons \text{HO}_2 \quad K_7 = \alpha_{11} / \alpha_4 \sqrt{\alpha_6} \sqrt{p} \\ c_7 = K_7 \sqrt{p} \quad \alpha_{11} = c_7 \alpha_4 \sqrt{\alpha_6} \quad (12g)$$

$$\text{NO} + 1/2\text{O}_2 \rightleftharpoons \text{NO}_2 \quad K_8 = \alpha_{12} / \alpha_{10} \sqrt{\alpha_4} \sqrt{p} \\ c_8 = K_8 \sqrt{p} \quad \alpha_{12} = c_8 \alpha_{10} \sqrt{\alpha_4} \quad (12h)$$

Here, p is the pressure (in atm), and K_1 – K_8 are the reaction equilibrium constants. In [55], reaction equilibrium constants are calculated from partial pressures (Table 1). For this, using curve fitting component partial pressures are expressed as a function of temperature as follows:

Table 1 Properties of natural gases [56, 57]

Components	NG01	Russian NG	Iran NG	Australian NG	US NG
CH4 (Methane) [mol%]	90.82	92.54	87.81	86.26	99.7
C2H6 (Ethane) [mol%]	4.97	4.47	4.09	8.23	0.09
C3H8 (Propane) [mol%]	2.93	1.97	1.25	3.26	0.03
C4H10 (Butane) [mol%]	1.01	0.95	0.87	0.96	0.01
N2 (Nitrogen) [mol%]	0.27	0.07	5.98	1.26	0.17

$$\log K_p = A \ln \left(\frac{T}{1000} \right) + \frac{B}{T} + C + DT + ET^2 \quad (13)$$

K_p values are calculated according to the JANAF tables [59]:

$$K_p = e^{-\frac{\Delta G^0}{RT}} \quad (14)$$

In addition to the eight reaction equations, from the atom balances of C, H, O and N extra four equations are used as follows:

$$C : \varepsilon\varphi X + b = (\alpha_1 + \alpha_5)N \quad (15)$$

$$H : \varepsilon\varphi Y = (2\alpha_2 + 2\alpha_6 + \alpha_7 + \alpha_9 + \alpha_{11})N \quad (16)$$

$$O : \varepsilon\varphi Z + 2a + 2b = (2\alpha_1 + \alpha_2 + 2\alpha_4 + \alpha_5 + \alpha_8 + \alpha_9 + \alpha_{10} + 2\alpha_{11} + 2\alpha_{12})N \quad (17)$$

$$N : \varepsilon\varphi Q + 2c = (2\alpha_3 + \alpha_{10})N \quad (18)$$

Here, α is the molar fractions of products and N is the total mole number of the products:

$$\alpha_k = \frac{\chi_k}{\sum_{k=1}^{12} \chi_k} \quad (19)$$

$$N = \sum_{k=1}^{12} \chi_k \quad (20)$$

Eventually, the total number of unknowns becomes 13. Thus, from the conservation of mass for given in Eq. (21) an extra equation is obtained to form a linear system. As a result, linear system has 13 equations for the 13 unknowns to be solved:

$$\sum_{k=1}^{12} \alpha_k - 1 = 0 \quad (21)$$

By dividing Eqs. (16)–(18) into Eq. (15), the following equations are obtained:

$$2\alpha_2 + 2\alpha_6 + \alpha_7 + \alpha_9 + \alpha_{11} - (\alpha_1 + \alpha_5) \frac{\varepsilon\varphi Y}{\varepsilon\varphi X + b} = 0 \quad (22)$$

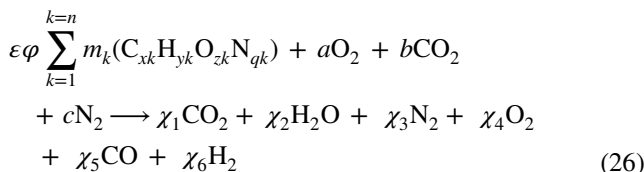
$$2\alpha_1 + \alpha_2 + 2\alpha_4 + \alpha_5 + \alpha_8 + \alpha_9 + \alpha_{10} + 2\alpha_{11} + 2\alpha_{12} - (\alpha_1 + \alpha_5) \frac{\varepsilon\varphi Z + 2a + 2b}{\varepsilon\varphi X + b} = 0 \quad (23)$$

$$2\alpha_3 + \alpha_{10} + \alpha_{12} - (\alpha_1 + \alpha_5) \frac{\varepsilon\varphi Q + 2c}{\varepsilon\varphi X + b} = 0 \quad (24)$$

Substituting Eqs. (12a)–(12h) into Eqs. (21)–(24), nonlinear equations of four and independent variables $\alpha_3, \alpha_4, \alpha_5,$ and α_6 are obtained [58]:

$$f_j = (\alpha_3, \alpha_4, \alpha_5, \alpha_6) = 0 \quad j = 1, 2, 3, 4 \quad (25)$$

Equation (25) can be solved with Newton–Raphson method to find the equilibrium mole fractions:



Firstly, initial values for iterative calculation are determined through solving, the chemical reaction equation for combustion at $T < 1000$ Eq. (26). In this case, there are six unknowns, combustion products given in Eq. (26), but four equations of atomic conservations. In the lean and stoichiometric combustion cases, $\chi_5 = \chi_6 = 0$ is considered, since CO and H_2 are oxidized. Thus, equation system is linear and can be solved. In the rich case, $\chi_4 = 0$ is considered, since all the O_2 is consumed. And introducing the water–gas reaction $H_2 + CO_2 \rightleftharpoons H_2O + CO$, one extra equation for the equilibrium constant is added. In this case, there are five unknowns, combustion products given in Eq. (26). The equation system has four equations of atomic conservations and one from the water–gas reaction equilibrium constant. Thus, equation system is linear and can be solved. In the lean combustion case, formation of products depends on equivalence ratio, not pressure and temperature. However, in the rich combustion case, formation of combustion products depends on pressure, temperature and equivalence ratio. The temperature dependent of the water–gas reaction equilibrium constant [58]:

$$\ln K = 2,743 - \frac{1}{T} \left[1761 - \frac{1611000}{T} + \frac{280300}{T^2} \right] \quad (27)$$

where the reaction temperature is denoted as T (in K). The constant pressure equilibrium constant can be defined as follows:

$$K = \frac{\chi_2 \chi_5}{\chi_1 \chi_6} \quad (28)$$

Reaction constant χ_5 is solved by substituting Eq. (28) into Eq. (27) from the resulting quadratic equation. In the end, to initialize iterative calculations $\alpha_3^{(1)}, \alpha_4^{(1)}, \alpha_5^{(1)}$ and $\alpha_6^{(1)}$ are determined. By iterating Eq. (25) neglecting the second and higher grade derivatives and expanding into Taylor series the following four equations are obtained and $\Delta\alpha_k$ is found:

$$f_j + \frac{\partial f_j}{\partial \alpha_3} \Delta \alpha_3 + \frac{\partial f_j}{\partial \alpha_4} \Delta \alpha_4 + \frac{\partial f_j}{\partial \alpha_5} \Delta \alpha_5 + \frac{\partial f_j}{\partial \alpha_6} \Delta \alpha_6 \cong 0 \quad j = 1, 2, 3, 4 \quad (29)$$

where

$$\Delta \alpha_k = \alpha_k^* - \alpha_k^{(1)} \quad (30)$$

Equations in Eq. (29), explicitly, in matrix notation are as follows:

$$\begin{bmatrix} f_1(\alpha_3^{(1)}, \alpha_4^{(1)}, \alpha_5^{(1)}, \alpha_6^{(1)}) \\ f_2(\alpha_3^{(1)}, \alpha_4^{(1)}, \alpha_5^{(1)}, \alpha_6^{(1)}) \\ f_3(\alpha_3^{(1)}, \alpha_4^{(1)}, \alpha_5^{(1)}, \alpha_6^{(1)}) \\ f_4(\alpha_3^{(1)}, \alpha_4^{(1)}, \alpha_5^{(1)}, \alpha_6^{(1)}) \end{bmatrix} + \begin{bmatrix} \text{Results} \\ \text{of} \\ \text{Jacobian} \\ \text{Matrix} \end{bmatrix} \times \begin{bmatrix} \Delta \alpha_3 \\ \Delta \alpha_4 \\ \Delta \alpha_5 \\ \Delta \alpha_6 \end{bmatrix} \cong 0 \quad (31)$$

Using Eqs. (30), (31) can be solved iteratively. Intermediate iteration steps can be solved as follows:

$$\alpha_k^{(2)} = \alpha_k^{(1)} + \Delta \alpha_k \quad k = 3, 4, 5, 6 \quad (32)$$

The iterative solution of equation system is proceeded up to a certain tolerance value of $|\Delta \alpha_k|$. The unknowns, α_3 , α_4 , α_5 , and α_6 , are obtained by solving the values lower than the desired tolerance. The rest of the unknowns are calculated by substituting the solved ones into equations of Eqs. (12a)–(12h). Eventually, the unknowns of molar fractions at equilibrium are calculated.

At high temperatures combustion products undergo thermal disassociations, this also affects specific heats. This requires calculation of changes in combustion species mole fraction with temperature. Partial derivative of Eq. (25) with respect to temperature can be calculated:

$$\frac{\partial f_j}{\partial T} + \frac{\partial f_j}{\partial \alpha_3} \frac{\partial \alpha_3}{\partial T} + \frac{\partial f_j}{\partial \alpha_4} \frac{\partial \alpha_4}{\partial T} + \frac{\partial f_j}{\partial \alpha_5} \frac{\partial \alpha_5}{\partial T} + \frac{\partial f_j}{\partial \alpha_6} \frac{\partial \alpha_6}{\partial T} = 0 \quad (33)$$

The similar procedure given for Eqs. (29)–(32) can be followed to solve Eq. (33). The specific heats of combustion products can be calculated using Eq. (41) with the results obtained.

Using the coefficients ($a_1 \dots a_n$), enthalpies in Eq. (35), molar specific heats in Eq. (35) and entropies in Eq. (36) for the corresponding species can be calculated [60]:

$$\frac{\bar{h}_k}{R_u T} = a_{1,k} + \frac{a_{2,k}}{2} T + \frac{a_{3,k}}{3} T^2 + \frac{a_{4,k}}{4} T^3 + \frac{a_{5,k}}{5} T^4 + \frac{a_{6,k}}{2} \quad (34)$$

$$\frac{\bar{c}_{p,k}}{R_u} = a_{1,k} + a_{2,k} T + a_{3,k} T^2 + a_{4,k} T^3 + a_{5,k} T^4 \quad (35)$$

$$\frac{\bar{s}_k^0}{R_u T} - a_{1,k} \ln T + a_{2,k} T + \frac{a_{3,k}}{2} T^2 + \frac{a_{4,k}}{2} T^3 + \frac{a_{5,k}}{2} T^4 + a_{7,k} \quad (36)$$

The enthalpy of the mixture can be calculated considering the temperature change at constant pressure. The ultimate thermodynamic properties of the product gases there are as follows:

$$\bar{h} = \sum_{k=1}^{12} \alpha_k \bar{h}_k \quad (37)$$

$$h = \frac{1}{M} \sum_{k=1}^{12} \alpha_k \bar{h}_k \quad (38)$$

$$\bar{s} = \frac{R_u}{M} \left[\sum_{k=1}^n \alpha_k (\bar{s}_k^0 - \ln \alpha_k) - \ln \left(\frac{P}{P_0} \right) \right] \quad (39)$$

$$\left(\frac{\partial h}{\partial T} \right)_P = c_{p_g} = \sum_{k=1}^{12} \frac{\alpha_k}{M} \frac{\partial \bar{h}_k}{\partial T} + \frac{\bar{h}_k}{M} \frac{\partial \alpha_k}{\partial T} - \frac{\alpha_k \bar{h}_k}{M^2} \frac{\partial M}{\partial T} \quad (40)$$

Using Eqs. (34)–(38) and rearranging Eq. (29), the following expression is obtained:

$$\left(\frac{\partial h}{\partial T} \right)_P = c_{p_g} = \frac{1}{M} \left[\sum_{k=1}^{12} \alpha_k \bar{c}_{p,k} + \bar{h}_k \frac{\partial \alpha_k}{\partial T} - h M_T \right] \quad (41)$$

$$M_T = \frac{\partial M}{\partial T} = \sum_{k=1}^{12} M_k \frac{\partial \alpha_k}{\partial T} \quad (42)$$

Here, the combustion temperature is T (in K). The product molar mass is M_k , and the total products molar mass is M .

$$M = \sum_{k=1}^{12} m_k = \sum_{k=1}^{12} \alpha_k M_k \quad (43)$$

The total mass of products (m_p) is equal to the total mass (m_R) of the reactants. And, the total number of moles of the products can be found from the following equation:

$$N = \frac{m_{\text{fuel}} + m_{\text{CO}_2} + m_{\text{O}_2} + m_{\text{N}_2}}{M} \quad (44)$$

Finally, mole numbers $\chi_1, \chi_2, \chi_3, \dots, \chi_n$ of the products are found as follows:

$$\chi_k = \alpha_k N \quad (45)$$

The adiabatic flame temperature is solved iteratively. Iteration is initialized with an estimated temperature. Iteration is followed up to an adequate temperature tolerance (10^{-6}). So, it is expressed as follows:

$$\Delta T = \frac{(h_r - h_p)}{c_p} \tag{46}$$

where c_p is calculated by Eq. (41), h_r is the enthalpy of reactants, and h_p is the enthalpy of products. With the iterations to be made, the adiabatic flame temperature (AFT) is found with minimum error:

$$AFT^{n+1} = AFT^n + \Delta T \tag{47}$$

3 Results and Discussion

Thermodynamic analysis of oxy-fuel combustion has been conducted according to the above procedure. In Figs. 2, 3, 4, 5 and 6 change of adiabatic flame temperature, specific heat, entropy, NOx emissions and concentration of combustion products are presented for varying equivalence ratio, combustion chamber inlet temperature, combustion pressure and oxygen rates.

Figure 2a–d shows the effects of the change of the equivalence ratio on the adiabatic flame temperature, NOx emissions, specific heat, and entropy values. As shown in Fig. 2a, when the adiabatic flame temperature changes with the variation of the equivalence ratio from 0.3 to 1.5 it can be seen that the characteristic of conventional combustion

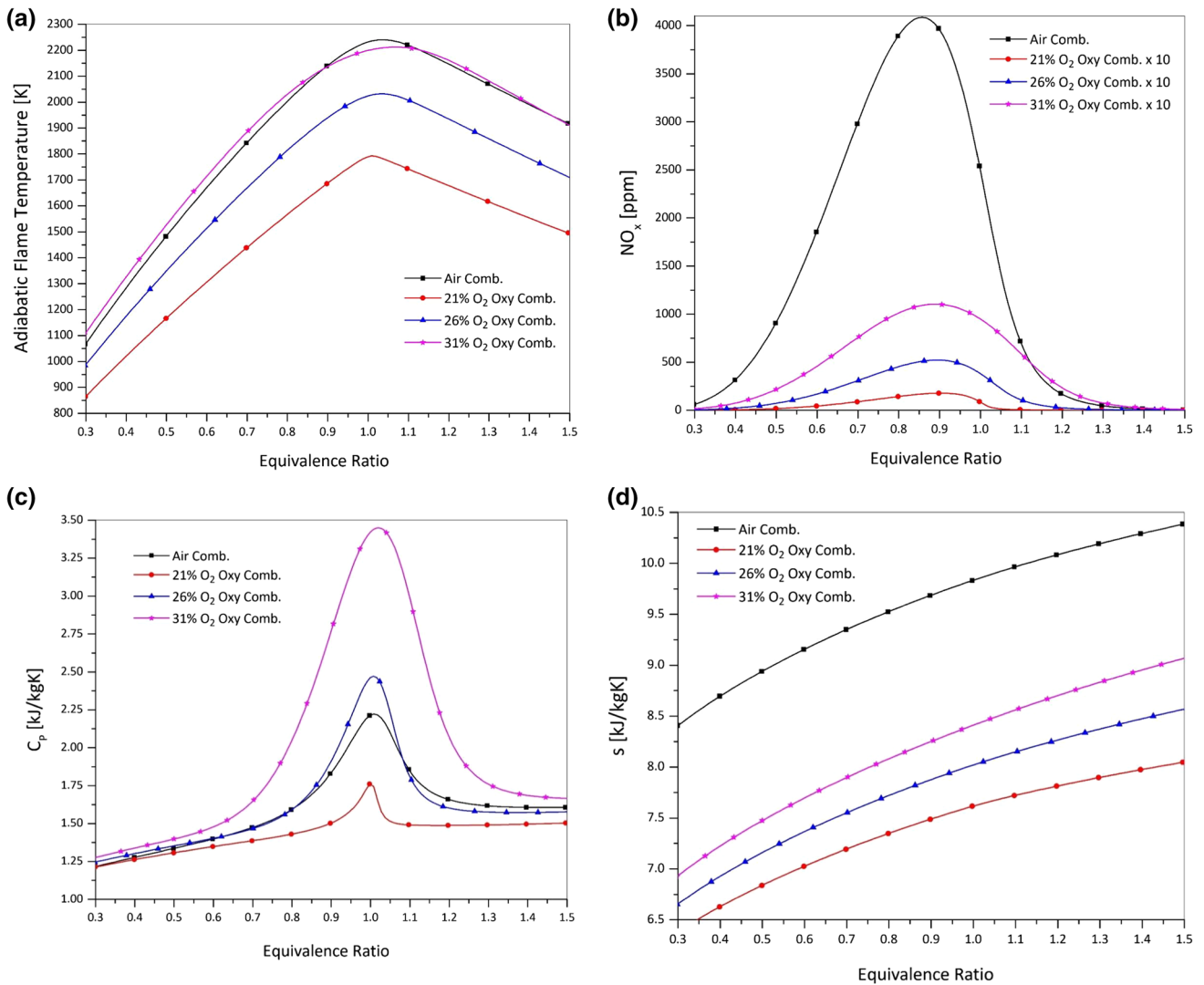


Fig. 2 Adiabatic flame temperatures (a), NOx emissions (b), constant pressure specific heats (c) and entropies (d) with equivalence ratio for various oxygen fractions. ($P=1$ atm, $T_i=300$ K)

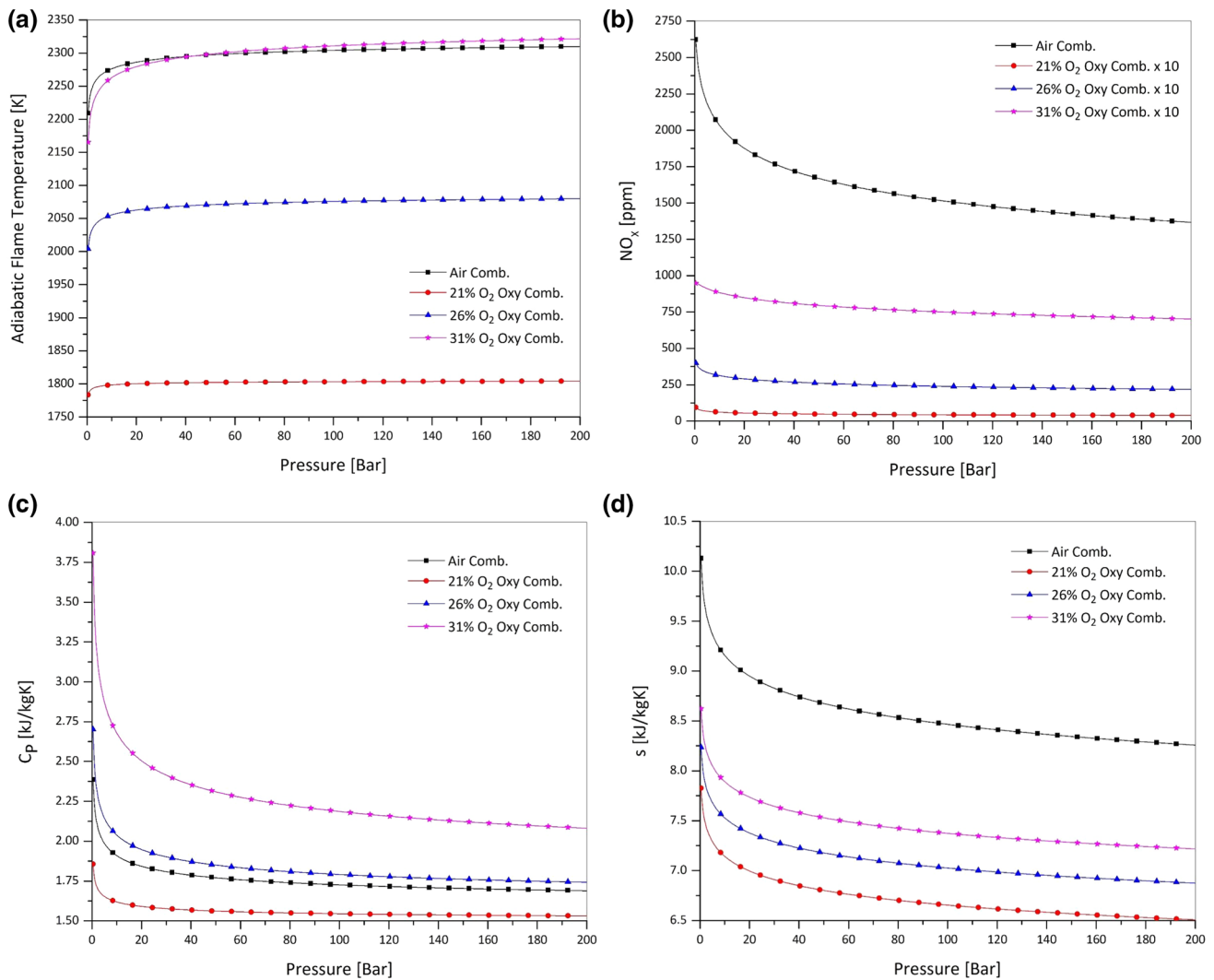


Fig. 3 Adiabatic flame temperatures (a), NO_x emissions (b), constant pressure specific heats (c) and entropies (d) with pressure for various oxygen fractions. ($\phi=1$, $T_i=305$ K)

has a very similar characteristic with the characteristic of oxy-combustion of 31% oxygen. The figure also shows that oxy-combustion of 26% oxygen gives lower flame temperatures compared to these two conditions, but it gives higher results than oxy-combustion with a ratio of 21% oxygen. Inlet temperature of turbine is determined by the blade material strength at dedicated temperatures. Accordingly, fuel consumption at that specific temperature will be higher for lower oxygen ratios. Figure 2b presents that combustion with air results in 40 times more emissions than oxy-combustion with 31% oxygen content. It is also obvious that NO_x emissions from conventional combustion are much more than that of oxy-combustions at all oxygen fractions. In Fig. 2c specific heats are compared at varying oxygen ratios. Results show that oxy-combustion with a ratio of 31% and 26% has higher specific heat ratios which is an advantage in terms of net power production

of the cycle. The conventional combustion condition is almost similar to the 26% oxy-combustion rate until the equivalence ratio reaches 0.8. At ratios between 0.8 and 1.1, the air combustion has lower specific heat values than 26% oxy-combustion. On the other hand, oxy-combustion with 21% oxygen is more advantageous overall. Having examined in terms of entropy, another order is seen to be occurred (Fig. 2d). In other words, in the case of conventional combustion, the entropy value was determined to be almost one and a half times of oxy-combustion with a ratio of 21% oxygen. As the percentage of oxygen in oxy-combustion increases from 21 to 31%, entropy also increases. However, oxy-combustion results in lower entropy values than conventional combustion in all cases. As entropy is lower in oxy-combustion, exergy potential is higher than that of conventional combustion. As entropy is lower in oxy-combustion, exergy potential of the CC

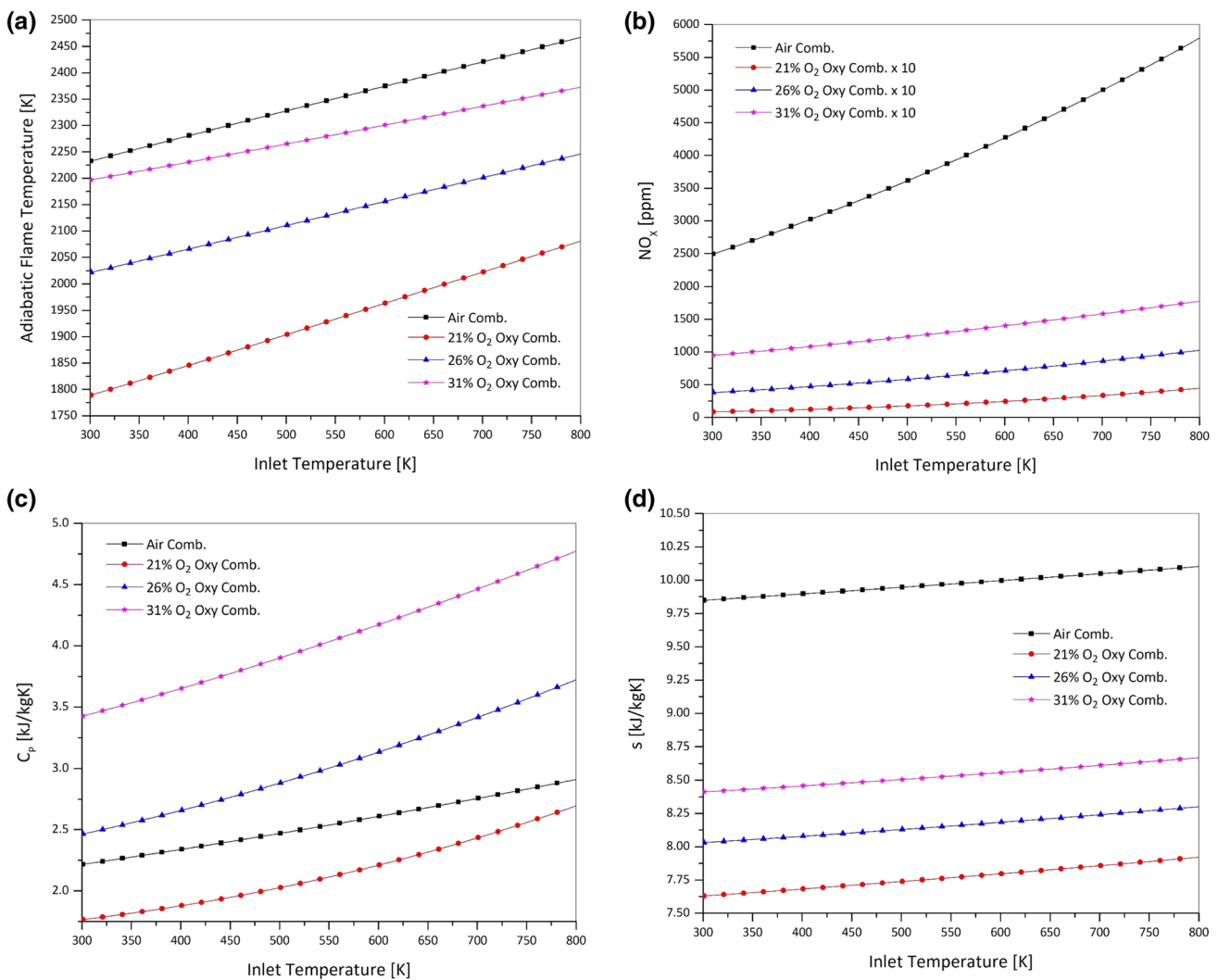


Fig. 4 Adiabatic flame temperatures (a), NOx emissions (b), constant pressure specific heats (c) and entropies (d) with inlet temperature for various oxygen fractions. ($\phi = 1, P = 1$ atm)

exhaust is higher than that of conventional combustion which would result higher reversible work obtained from the power turbine.

Figure 3a–d shows the effect of change in the combustion pressure, on the adiabatic flame temperature, NOx emissions, specific heat, and entropy values. Besides the equivalence ratio, combustion pressure is also very important for combustion. Compressor pressure ratios in today’s thermal power plants are around 30. In oxy-fuel power plants, the pressure value is more than 74 bar in cycles such as supercritical CO₂ cycle. (CO₂ behaves as a supercritical fluid above its critical temperature 30.98 °C and critical pressure 73.8 bar [61]) Referring to Fig. 3a, there is an increasing trend for adiabatic flame temperature due to the change in combustion pressure between 1 and 4 bar, while there is only a slight increase in the adiabatic flame temperature above 20 bar. This increase is 15 K in oxy-combustion with the

ratio of 21% oxygen from 1 to 200 bar, 60 K for 26% and 130 K for oxy-combustion with the ratio of 31%. When NOx emissions, specific heat, and entropy values are examined, it is seen that all decrease with increasing pressure as shown in Fig. 3b–d.

One of the most important parameters for combustion in power generation plants is the temperature of the oxidant and fuel mixture entering the combustion chamber in Fig. 4a–d. As the combustion chamber inlet temperature increases, the adiabatic flame temperature increases in all cases. For all inlet temperatures, conventional combustion is more advantageous than oxy-combustion. In conventional combustion, when the inlet temperature is increased from 300 to 800 K the adiabatic flame temperature increases by 234 K, while by 291 K, 224 K and 176 K at oxy-combustion with 21%, 26%, and 31% oxygen, respectively. Depending on the compression ratio in thermal power plants, when the

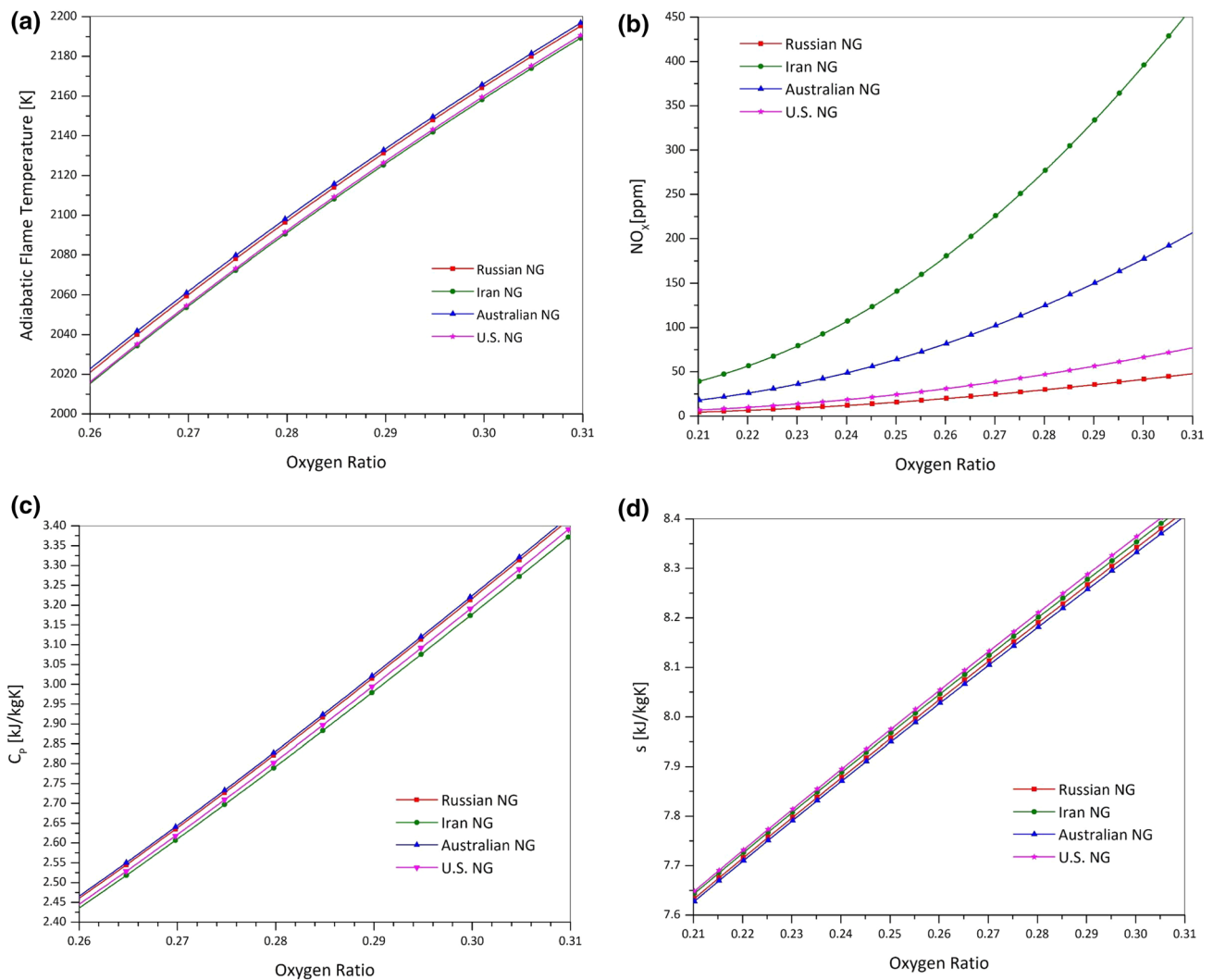


Fig. 5 Adiabatic flame temperatures (a), NO_x emissions (b), constant pressure specific heats (c) and entropies (d) with oxygen ratio of oxy-combustion for four different natural gas origins. ($\phi = 1$, $P = 1$ atm, $T_i = 300$ K)

inlet temperature is changed from 300 to 800 K, the NO_x emissions increase by 230%. In oxy-combustion power plants, when the inlet temperature is changed from 300 to 800 K by incorporating the gases in the exhaust into the recirculation with recuperator, heat exchanger, etc.; 400%, 300%, 200% increase in emissions is seen for 21%, 26% and 31% oxygen ratios, respectively. Moreover, even in the case of the oxy-combustion, for the highest value obtained, NO_x emissions are 1/130 of the obtained quantity from conventional combustion.

According to the figures, the effect of inlet temperature in terms of specific heat, the specific heat increase in conventional combustion is observed to be about half of that of oxy-combustions. This result is opposite in terms of entropy; namely, it is found that the increase in entropy with the combustion inlet temperature for conventional combustion is the least. Also, it is observed that 31% oxy-combustion

presented a lower entropy increase than oxy-combustion of 26% and 21% oxygen ratios.

This study is conducted on a single natural gas mixture up to this section. However, the content of natural gas components varies according to the location of drilling [56, 57]. The results of the analysis of the natural gas of Russia, Iran, Australia and the USA which are one of the prominent natural gases of the world reserve are shown in Fig. 5a–d. When these four different natural gases are examined, adiabatic flame temperature and specific heat increase logarithmically with the oxygen ratio. In terms of adiabatic flame temperature and specific heat it is concluded that the most advantageous natural gases are Australian, Russian, USA and Iran, respectively. On the other hand, in terms of entropy, it is seen that the order of priority is Australian, Russian, Iranian and USA natural gas. Considering the NO_x emission results, it is determined that Iranian natural gas emission values

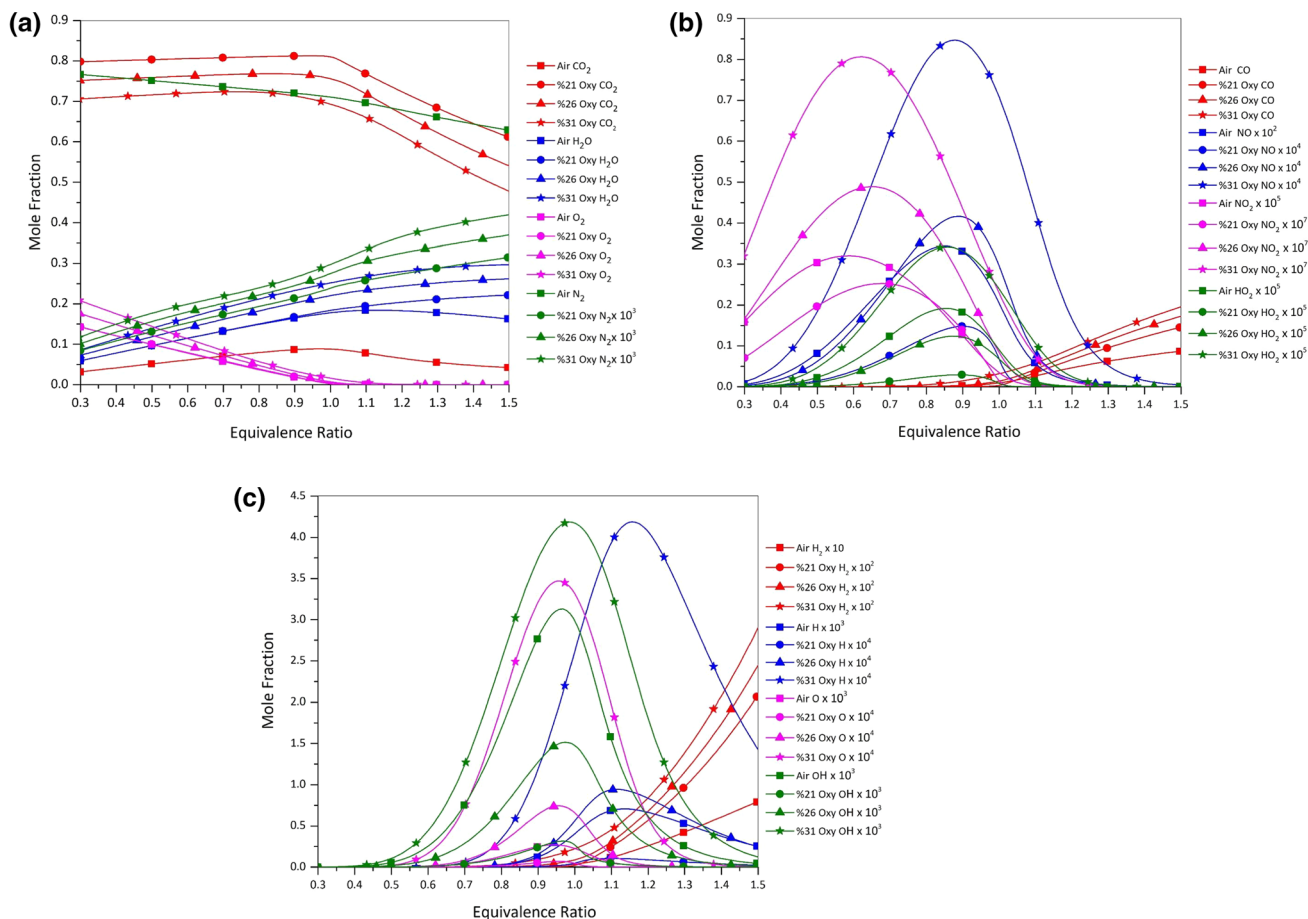


Fig. 6 CO_2 , H_2O , N_2 , O_2 molar fractions (a), CO , NO , NO_2 , HO_2 molar fractions (b), O , H_2 , H , OH molar fractions (c) with equivalence ratio for various oxygen fractions. ($T_i = 300 \text{ K}$, $P = 1 \text{ atm}$)

are more than the others. As a result, the natural gas to be used should be chosen regarding to a specific parameter. In another words, natural gas to be used should be decided by considering its pros and cons. The mole fractions of the combustion products are shown in Fig. 6a–c with different scales, for four different conditions as the conventional combustion with air and oxy-combustions with the oxygen ratios of 21%, 26% and 31% according to the equivalence ratio.

Results are validated with two popular combustion programs NASA CEA and GASEQ, and the accuracy of the results of the combustion model are presented in Tables 2, 3, 4 and 5 for four different cases (i.e., at different inlet pressure, inlet temperature and equivalence ratios) and Fig. 7 for 30 arbitrary cases. In Fig. 7, the mean difference and maximum difference from the results obtained from NASA CEA and GASEQ are shown. In Fig. 7, calculated results are very close to the CEA program results, differences in adiabatic flame temperatures are about 0.01%, enthalpies are about 0.07%, and entropies are about 0.006%. The similar comparison with the GASEQ program are about 0.02%, 0.05%, and 0.01%,

respectively. The mean differences for molar fractions of CO_2 , O_2 , H_2O , and N_2 are well below 0.4%. The differences in eight of combustion products (CO_2 , H_2O , N_2 , O_2 , CO , O , H_2 , H) are very low, while the rest (NO , NO_2 , HO_2 , OH) are higher. Thus, slight differences in results are present. However, the differences in the constant pressure specific heats differ from the GASEQ program, considerably. This is because GASEQ neglects effects of dissociations on the specific heat of the combustion products. For this reason specific heat results obtained from GASEQ and CEA differ significantly especially at high temperatures. Therefore, it is strongly recommended for researchers to use CEA or an equilibrium model when calculating taking thermal dissociations into account. GASEQ calculates the specific heat directly from Eq. (35) instead of calculating derivatives and using Eq. (40). The deviations of model results both from GASEQ and NASA CEA for HO_2 are as high as %33. The reason for this deviation is meticulously investigated. Same method which gives only around %0.4 error is applied to HO_2 with JANAF

Table 2 Combustion results for conventional combustion in comparison with CEA and GASEQ programs

$(P = 1 \text{ atm, } T_u = 300 \text{ K, } \phi = 1) \text{ air combustion}$					
	CEA	GASEQ	MODEL	CEA deviations (%)	GASEQ deviations (%)
Tady (K)	2231	2232.5	2232.5	-0.0672	0.0000
C_p (kJ/kg K)	2.2121	1.50372	2.21138	0.0326	-32.0008
h (kJ/kg)	-235.87	-236.77	-236.52	-0.2748	0.1057
s (kJ/kg K)	9847.3	9846.44	9847.05	0.0025	-0.0062
N_2	0.71064	0.71059	0.710618	0.0031	-0.0039
H_2O	0.17778	0.17787	0.177805	-0.0141	0.0366
CO_2	0.08807	0.08809	0.088157	-0.0987	-0.0760
CO	0.00945	0.00942	0.0094179	0.3408	0.0223
O_2	0.00471	4.79E-03	0.00475	-0.8421	0.8421
OH	0.003124	2.99E-03	0.003007	3.8909	-0.5653
H	0.0004	4.01E-04	0.000403	-0.7444	-0.4963
O	0.00022	2.27E-04	0.000223	-1.3453	1.7937
H_2	0.00355	3.57E-03	0.003583	-0.9210	-0.3628
NO	0.00198	2.01E-03	0.002	-1.0000	0.3000
NO_2		3.50E-07	3.55E-07		-1.4085
HO_2		6.47E-07	8.16E-07		-20.7108

Table 3 Combustion results for %21 O_2 oxy-combustion in comparison with CEA and GASEQ programs

$(P = 1 \text{ atm, } T_u = 300 \text{ K, } \phi = 0.9) \text{ \%21 } O_2 \text{ oxy-combustion}$					
	CEA	GASEQ	MODEL	CEA deviations (%)	GASEQ deviations (%)
Tady (K)	1686.7	1688.4	1686.7	0.0000	0.1008
C_p (kJ/kg K)	1487.3	1448.09	1501.45	-0.9424	-3.5539
h (kJ/kg)	-7374.37	-7375.4	-7375.63	-0.0171	-0.0031
s (kJ/kg K)	7502.6	7504.72	7503.23	-0.0084	0.0199
N_2	0.00021	2.08E-04	2.12E-04	-0.9434	-1.8868
H_2O	0.16747	0.16766	0.16742	0.0299	0.1434
CO_2	0.81234	0.81236	0.81231	0.0037	0.0062
CO	0.00034	3.47E-04	0.0003426	-0.7589	1.2843
O_2	0.01933	1.91E-02	1.93E-02	0.2593	-0.7261
OH	0.00026	2.44E-04	2.54E-04	2.3622	-3.9370
H		6.01E-07	5.93E-07		1.2985
O	0.00001	5.41E-06	5.38E-06	0.3717	0.5576
H_2	0.00002	2.14E-05	2.10E-05	0.0000	1.9048
NO	0.00001	1.45E-05	1.48E-05	-1.3514	-2.0270
NO_2		1.34E-08	1.36E-08		-1.4706
HO_2		2.62E-07	2.90E-07		-9.6552

table data, and three different dissociation reactions are considered: $O_2 + 1/2H_2 \rightleftharpoons HO_2$, $O_2 + H \rightleftharpoons HO_2$ and $O + OH \rightleftharpoons HO_2$. Eventually, HO_2 mol fractions are

similar in GASEQ and CEA programs because the calculations are based on the same fundamental methods. Moreover, the present model results are consistent with the programs compared.

Table 4 Combustion results for %26 O₂ oxy-combustion in comparison with CEA and GASEQ programs

($P = 1 \text{ atm}$, $T_u = 300 \text{ K}$, $\phi = 0.9$) %26 O₂ oxy-combustion

	CEA	GASEQ	MODEL	CEA deviations (%)	GASEQ deviations (%)
Tady (K)	2004.9	2005.6	2004.9	0.0000	0.0349
C_p (kJ/kg K)	1729.8	1540.76	1787.93	-3.2512	-13.8244
h (kJ/kg)	-6963.9	-6965.27	-6964.9	-0.0144	0.0053
s (kJ/kg K)	8158.9	8160.04	8159.6	-0.0086	0.0054
N ₂	0.0003	2.97E-04	3.00E-04	0.0000	-1.0000
H ₂ O	0.23407	0.23416	0.23409	-0.0085	0.0299
CO ₂	0.71817	0.71795	0.71835	-0.0251	-0.0557
CO	0.04297	0.043314	0.043117	-0.3409	0.4569
O ₂	0.00052	5.16E-04	0.000519	0.1927	-0.5780
OH	0.00081	7.30E-04	0.000767	5.6063	-4.8240
H	0.00009	9.33E-05	9.35E-05	-0.5348	-0.2139
O	0.00002	1.57E-05	1.61E-05	-0.6211	-2.4845
H ₂	0.00305	3.08E-03	3.06E-03	-0.3268	0.6536
NO	0.00001	7.95E-06	8.10E-06	-1.2346	-1.8519
NO ₂		6.29E-10	6.30E-10		-0.1587
HO ₂		6.66E-08	8.53E-08		-21.9812

Table 5 Combustion results for %31 O₂ oxy-combustion in comparison with CEA and GASEQ programs

($P = 1 \text{ atm}$, $T_u = 300 \text{ K}$, $\phi = 1.2$) %31 O₂ oxy-combustion

	CEA	GASEQ	MODEL	CEA deviations (%)	GASEQ deviations (%)
Tady (K)	2156.87	2158.6	2156.87	0.0000	0.0802
C_p (kJ/kg K)	1944.3	1942.8144	2016.05	-3.5589	-3.6326
h (kJ/kg)	-6561.93	-6563.62	-6563.28	-0.0206	0.0052
s (kJ/kg K)	8701.7	8701.9	8701.4	0.0034	0.0057
N ₂	0.00036	3.58E-04	3.61E-04	-0.2770	-0.8310
H ₂ O	0.27985	0.27989	0.27954	0.1109	0.1252
CO ₂	0.61442	0.61455	0.61445	-0.0049	0.0163
CO	0.09379	0.09369	0.09338	0.4391	0.3320
O ₂	0.00084	8.48E-04	0.00084	0.0000	0.9524
OH	0.00196	1.80E-03	0.00186	5.3763	-3.2258
H	0.0004	4.04E-04	4.05E-04	-1.2346	-0.2469
O	0.00006	5.97E-05	5.92E-05	1.3514	0.8446
H ₂	0.00832	8.38E-03	0.00835	-0.3593	0.3593
NO	0.00002	1.64E-05	1.65E-05	3.0303	-0.6061
NO ₂		1.31E-09	1.32E-09		-0.7576
HO ₂		1.63E-07	2.10E-07		-22.3810

4 Conclusion

In this study, a novel equilibrium combustion model is modified for oxy-fuel combustion in order to obtain adiabatic flame temperature, mole fractions and thermodynamic properties of combustion products for varying

oxygen ratios. Natural gases from four important origins (Russia, USA, Iran, Australia) are considered, and the results of the analysis are validated with CEA and GASEQ software. It has been seen that, in terms of adiabatic flame temperature, conventional combustion has similar characteristics for 31% O₂ oxy-combustion and provided higher results than that of oxy-combustion of 26% O₂ and 21% O₂.

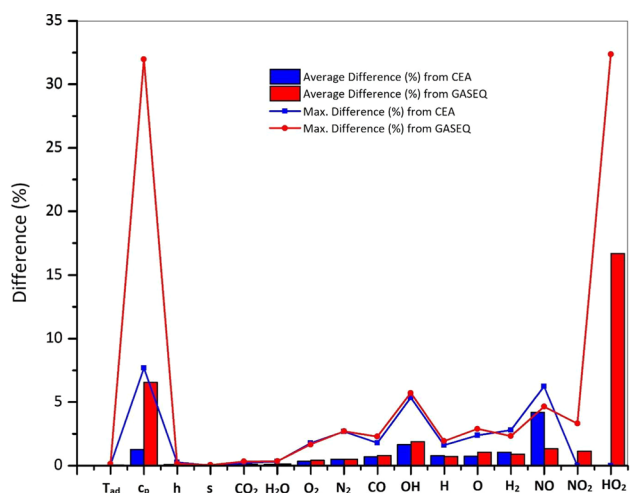


Fig. 7 Comparison of model results with results (Difference % = [(Program value – Model Value)/(Model Value) × 100])

But for the specific heat constant (c_p), conventional combustion values are closer to c_p values of oxy-combustion with 26% O₂ and provided higher results than that of oxy-combustion of 21% O₂ and 31% O₂. Also, it is concluded that the entropy values in oxy-combustion are significantly reduced in comparison with the results of the conventional combustion. As the oxygen content in the oxy-combustion is increased, the entropy is increased. Lower entropy production of oxy-combustion is an indication of higher exergy potential of the CC exhaust which would result higher reversible work obtained from the power turbine. In terms of emissions, oxy-combustion power plants have been used for carbon capture and storage (CCS) with zero CO₂ emissions. This study presents that oxy-combustion also produces much fewer NO_x emissions than air combustion in the order of below 1/40. Analysis of natural gases of different resources shows that thermodynamic properties vary from source to source. In terms of adiabatic flame temperature, specific heat, and entropy, Australian natural gas showed better results among the tested fuels, while Russian natural gas emits least NO_x emissions. On the other hand, using Iranian natural results the lowest adiabatic flame temperature and specific heat but highest NO_x emissions. In terms of entropy the highest values are obtained from US natural gas. The mole fractions of the combustion products have been evaluated for four different conditions both for conventional combustion and oxy-combustions.

Acknowledgements This work is compiled from the first author's unpublished PhD dissertation. We would like to thank the Turkish Academy of Sciences (TUBA-GEBIP) and The Scientific and Technological Research Council of Turkey (TUBITAK) for their support for graduate students.

References

- Mletzko, J.; Ehlers, S.; Kather, A.: Comparison of natural gas combined cycle power plants with post combustion and oxyfuel technology at different CO₂ capture rates. *Energy Procedia* **86**, 2–11 (2016). <https://doi.org/10.1016/j.egypro.2016.01.001>
- Choi, B.S.; Kim, M.J.; Ahn, J.H.; Kim, T.S.: Influence of a recuperator on the performance of the semi-closed oxy-fuel combustion combined cycle. *Appl. Therm. Eng.* **124**, 1301–1311 (2017). <https://doi.org/10.1016/j.applthermaleng.2017.06.055>
- Zhao, Y.; Chi, J.; Zhang, S.; Xiao, Y.: Thermodynamic study of an improved MATIANT cycle with stream split and recompression. *Appl. Therm. Eng.* **125**, 452–469 (2017). <https://doi.org/10.1016/j.applthermaleng.2017.05.023>
- Mathieu, P.; Nihart, R.: Zero-Emission MATIANT Cycle. International Gas Turbine and Aeroengine Congress and Exhibition
- Allam, R.J.; Freed, D.A.; Fetvedt*, J.E.; Forrest, B.A.: The oxy-fuel supercritical CO₂ allam cycle: new cycle developments to produce even lower-cost electricity from fossil fuels without atmospheric emissions. In: Proceedings of ASME Turbo Expo 2014: Turbine Technical Conference and Exposition GT2014. (2014)
- Scaccabarozzi, R.; Gatti, M.; Martelli, E.: Thermodynamic analysis and numerical optimization of the NET Power oxy-combustion cycle. *Appl. Energy* **178**, 505–526 (2016). <https://doi.org/10.1016/j.apenergy.2016.06.060>
- Allam, R.; Martin, S.; Forrest, B.; Fetvedt, J.; Lu, X.; Freed, D.; Brown, G.W.; Sasaki, T.; Itoh, M.; Manning, J.: Demonstration of the allam cycle: an update on the development status of a high efficiency supercritical carbon dioxide power process employing full carbon capture. *Energy Procedia* **114**, 5948–5966 (2017). <https://doi.org/10.1016/j.egypro.2017.03.1731>
- Scaccabarozzi, R.; Gatti, M.; Martelli, E.: Thermodynamic optimization and part-load analysis of the NET power cycle. *Energy Procedia* **114**, 551–560 (2017). <https://doi.org/10.1016/j.egypro.2017.03.1197>
- Allama, R.J.; Palmer, M.R.; Brown Jr., G.W.; Fetvedt, J.; Freed, D.; Nomoto, H.; Itoh, M.; Okita, N.; Jones Jr., C.: High efficiency and low cost of electricity generation from fossil fuels while eliminating atmospheric emissions, including carbon dioxide
- Tsatsaronis, G.; Penkuhn, M.: Exergy Analysis of the allam cycle. In: The 5th International Symposium: Supercritical CO₂ Power Cycles March 28–31, 2016, San Antonio, Texas
- Sanz, W.; Jericha, H.; Moser, M.; Heitmeir, F.: Thermodynamic and economic investigation of an improved graz cycle power plant for CO₂ capture. *J. Eng. Gas Turbin. Power* **127**, 765 (2005). <https://doi.org/10.1115/1.1850944>
- Ferrari, N.; Mancuso, L.; Davison, J.; Chiesa, P.; Martelli, E.; Romano, M.C.: Oxy-turbine for Power Plant with CO₂ Capture. *Energy Procedia* **114**, 471–480 (2017). <https://doi.org/10.1016/j.egypro.2017.03.1189>
- Chowdhury, A.S.M.A.; Bugarin, L.; Badhan, A.; Choudhuri, A.; Love, N.: Thermodynamic analysis of a directly heated oxyfuel supercritical power system. *Appl. Energy* **179**, 261–271 (2016). <https://doi.org/10.1016/j.apenergy.2016.06.148>
- Skorek-Osikowska, A.; Bartela, L.; Kotowicz, J.: A comparative thermodynamic, economic and risk analysis concerning implementation of oxy-combustion power plants integrated with cryogenic and hybrid air separation units. *Energy Convers. Manag.* **92**, 421–430 (2015). <https://doi.org/10.1016/j.enconman.2014.12.079>
- Rogalev, A.; Rogalev, N.; Kindra, V.; Osipov, S.: Dataset of working fluid parameters and performance characteristics for the oxy-fuel, supercritical CO₂ cycle. *Data Brief.* **27**, 104682 (2019). <https://doi.org/10.1016/j.dib.2019.104682>



16. Habib, M.A.; Imteyaz, B.; Nemitallah, M.A.: Second law analysis of premixed and non-premixed oxy-fuel combustion cycles utilizing oxygen separation membranes. *Appl. Energy* (2019). <https://doi.org/10.1016/j.apenergy.2019.114213>
17. Jin, B.; Zhao, H.; Zou, C.; Zheng, C.: Comprehensive investigation of process characteristics for oxy-steam combustion power plants. *Energy Convers. Manag.* **99**, 92–101 (2015). <https://doi.org/10.1016/j.enconman.2015.04.031>
18. Rogalev, A.; Kindra, V.; Osipov, S.; Rogalev, N.: Thermodynamic analysis of the net power oxy-combustion cycle. In: Presented at the 13-th European Conference on Turbomachinery Fluid dynamics & Thermodynamics ETC13, Lausanne, Switzerland April 8 (2018)
19. Vega, F.; Camino, S.; Camino, J.A.; Garrido, J.; Navarrete, B.: Partial oxy-combustion technology for energy efficient CO2 capture process. *Appl. Energy* **253**, 113519 (2019). <https://doi.org/10.1016/j.apenergy.2019.113519>
20. Climent Barba, F.; Martínez-Denegri Sánchez, G.; Soler Seguí, B.; Gohari Darabkhani, H.; Anthony, E.J.: A technical evaluation, performance analysis and risk assessment of multiple novel oxy-turbine power cycles with complete CO2 capture. *J. Clean. Prod.* **133**, 971–985 (2016). <https://doi.org/10.1016/j.jclepro.2016.05.189>
21. Mehrpooya, M.; Zonouz, M.J.: Analysis of an integrated cryogenic air separation unit, oxy-combustion carbon dioxide power cycle and liquefied natural gas regasification process by exergoeconomic method. *Energy Convers. Manag.* **139**, 245–259 (2017). <https://doi.org/10.1016/j.enconman.2017.02.048>
22. Hong, J.; Field, R.; Gazzino, M.; Ghoniem, A.F.: Operating pressure dependence of the pressurized oxy-fuel combustion power cycle. *Energy* **35**, 5391–5399 (2010). <https://doi.org/10.1016/j.energy.2010.07.016>
23. Oki, Y.; Hamada, H.; Kobayashi, M.; Yuri, I.; Hara, S.: Development of High-efficiency Oxy-fuel IGCC System. *Energy Procedia* **114**, 501–504 (2017). <https://doi.org/10.1016/j.egypro.2017.03.1192>
24. Esquivel-Patiño, G.G.; Serna-González, M.; Nápoles-Rivera, F.: Thermal integration of natural gas combined cycle power plants with CO2 capture systems and organic Rankine cycles. *Energy Convers. Manag.* **151**, 334–342 (2017). <https://doi.org/10.1016/j.enconman.2017.09.003>
25. Mehrpooya, M.; Ansarinab, H.; Sharifzadeh, M.M.M.; Rosen, M.A.: Conventional and advanced exergoeconomic assessments of a new air separation unit integrated with a carbon dioxide electrical power cycle and a liquefied natural gas regasification unit. *Energy Convers. Manag.* **163**, 151–168 (2018). <https://doi.org/10.1016/j.enconman.2018.02.016>
26. Mehrpooya, M.; Sharifzadeh, M.M.M.; Katooli, M.H.: Thermodynamic analysis of integrated LNG regasification process configurations. *Prog. Energy Combust. Sci.* **69**, 1–27 (2018). <https://doi.org/10.1016/j.peecs.2018.06.001>
27. Mehrpooya, M.; Ghorbani, B.: Introducing a hybrid oxy-fuel power generation and natural gas/carbon dioxide liquefaction process with thermodynamic and economic analysis. *J. Clean. Prod.* **204**, 1016–1033 (2018). <https://doi.org/10.1016/j.jclepro.2018.09.007>
28. White, C.; Weiland, N.: Preliminary cost and performance results for a natural gas-fired direct sCO2 power plant. In: The 6th International Supercritical CO2 Power Cycles Symposium (2018)
29. Weiland, N.T.; White, C.W.: Techno-economic analysis of an integrated gasification direct-fired supercritical CO2 power cycle. In: 8th International Conference on Clean Coal Technologies (CCT2017) (2017)
30. Yantovski, E.I.; Zvagolsky, K.N.; Gavrilenko, E.A.: The cooperate: demo power cycle. *Energy Convers. Manag.* **36**, 861–864 (1995)
31. Xiang, Y.; Cai, L.; Guan, Y.; Liu, W.; Han, Y.; Liang, Y.: Study on the configuration of bottom cycle in natural gas combined cycle power plants integrated with oxy-fuel combustion. *Appl. Energy* **212**, 465–477 (2018). <https://doi.org/10.1016/j.apenergy.2017.12.049>
32. Gładysz, P.; Stanek, W.; Czarnowska, L.; Śladek, S.; Szłek, A.: Thermo-ecological evaluation of an integrated MILD oxy-fuel combustion power plant with CO2 capture, utilisation, and storage: A case study in Poland. *Energy* **144**, 379–392 (2018). <https://doi.org/10.1016/j.energy.2017.11.133>
33. Liu, M.; Lior, N.; Zhang, N.; Han, W.: Thermo-economic optimization of coolcep-s: a novel zero-CO2 emission power cycle using LNG (liquefied natural gas) coldness. In: 2008 ASME International Mechanical Engineering Congress and Exposition
34. Gładysz, P.; Ziębik, A.: Life cycle assessment of an integrated oxy-fuel combustion power plant with CO2 capture, transport and storage: Poland case study. *Energy* **92**, 328–340 (2015). <https://doi.org/10.1016/j.energy.2015.07.052>
35. Gładysz, P.; Stanek, W.; Czarnowska, L.; Węcel, G.; Langørgen, Ø.: Thermodynamic assessment of an integrated MILD oxyfuel combustion power plant. *Energy* **137**, 761–774 (2017). <https://doi.org/10.1016/j.energy.2017.05.117>
36. Farooqui, A.; Bose, A.; Ferrero, D.; Llorca, J.; Santarelli, M.: Techno-economic and exergetic assessment of an oxy-fuel power plant fueled by syngas produced by chemical looping CO2 and H2O dissociation. *J. CO2 Util.* **27**, 500–517 (2018). <https://doi.org/10.1016/j.jcou.2018.09.001>
37. Han, Y.; Cai, L.; Xiang, Y.; Guan, Y.; Liu, W.; Yu, L.; Liang, Y.: Numerical study of mixed working fluid in an original oxy-fuel power plant utilizing liquefied natural gas cold energy. *Int. J. Greenhouse Gas Control* **78**, 413–419 (2018). <https://doi.org/10.1016/j.ijggc.2018.09.013>
38. Ziółkowski, P.; Zakrzewski, W.; Kaczmarczyk, O.; Badur, J.: Thermodynamic analysis of the double Brayton cycle with the use of oxy combustion and capture of CO2. *Arch. Thermodyn.* **34**, 23–38 (2013). <https://doi.org/10.2478/aoter-2013-0008>
39. Weiland, N.T.; White, C.W.: Techno-economic analysis of an integrated gasification direct-fired supercritical CO2 power cycle. *Fuel* **212**, 613–625 (2018). <https://doi.org/10.1016/j.fuel.2017.10.022>
40. Crespi, F.; Gavagnin, G.; Sánchez, D.; Martínez, G.S.: Supercritical carbon dioxide cycles for power generation: a review. *Appl. Energy* **195**, 152–183 (2017). <https://doi.org/10.1016/j.apenergy.2017.02.048>
41. Zhao, Y.; Zhao, L.; Wang, B.; Zhang, S.; Chi, J.; Xiao, Y.: Thermodynamic analysis of a novel dual expansion coal-fueled direct-fired supercritical carbon dioxide power cycle. *Appl. Energy* **217**, 480–495 (2018). <https://doi.org/10.1016/j.apenergy.2018.02.088>
42. Crespi, F.; Gavagnin, G.; Sánchez, D.; Martínez, G.S.: Analysis of the thermodynamic potential of supercritical carbon dioxide cycles: a systematic approach. *J. Eng. Gas Turbin. Power* **140**, 051701 (2017). <https://doi.org/10.1115/1.4038125>
43. Strakey, P.A.: Oxy-combustion flame fundamentals for supercritical CO2 power cycles. In: The 6th International Supercritical CO2 Power Cycles Symposium (2018)
44. Liu, C.Y.; Chen, G.; Sipöcz, N.; Assadi, M.; Bai, X.S.: Characteristics of oxy-fuel combustion in gas turbines. *Appl. Energy* **89**, 387–394 (2012). <https://doi.org/10.1016/j.apenergy.2011.08.004>
45. Guan, Y.; Han, Y.; Wu, M.; Liu, W.; Cai, L.; Yang, Y.; Xiang, Y.; Chen, S.: Simulation study on the carbon capture system applying LNG cold energy to the O2/H2O oxy-fuel combustion. *Nat. Gas Ind. B* **5**, 270–275 (2018). <https://doi.org/10.1016/j.ngib.2017.11.011>
46. Liu, H.; Yao, H.; Yuan, X.; Xu, X.; Fan, Y.; Ando, T.; Okazaki, K.: Efficient desulfurization in O2/CO2 combustion: dependence on combustion conditions and sorbent properties. *Chem. Eng.*



- Commun. **199**, 991–1011 (2012). <https://doi.org/10.1080/00986445.2011.633288>
47. Han, S.H.; Lee, Y.S.; Cho, J.R.; Lee, K.H.: Efficiency analysis of air-fuel and oxy-fuel combustion in a reheating furnace. *Int. J. Heat Mass Transf.* **121**, 1364–1370 (2018). <https://doi.org/10.1016/j.ijheatmasstransfer.2017.12.110>
48. Shakeel, M.R.; Sanusi, Y.S.; Mokheimer, E.M.A.: Numerical modeling of oxy-methane combustion in a model gas turbine combustor. *Appl. Energy* **228**, 68–81 (2018). <https://doi.org/10.1016/j.apenergy.2018.06.071>
49. Kayadelen, H.K.; Ust, Y.: Prediction of equilibrium products and thermodynamic properties in H₂O injected combustion for $C\alpha H\beta O\gamma N\delta$ type fuels. *Fuel* **113**, 389–401 (2013). <https://doi.org/10.1016/j.fuel.2013.05.095>
50. Gonca, G.: Investigation of the influences of steam injection on the equilibrium combustion products and thermodynamic properties of bio fuels (biodiesels and alcohols). *Fuel* **144**, 244–258 (2015). <https://doi.org/10.1016/j.fuel.2014.12.032>
51. Kayadelen, H.K.: Effect of natural gas components on its flame temperature, equilibrium combustion products and thermodynamic properties. *J. Nat. Gas Sci. Eng.* **45**, 456–473 (2017). <https://doi.org/10.1016/j.jngse.2017.05.023>
52. Kayadelen, H.K.; Ust, Y.: Thermoenviromonic evaluation of simple, intercooled, STIG, and ISTIG cycles. *Int. J. Energy Res.* **42**, 3780–3802 (2018). <https://doi.org/10.1002/er.4101>
53. Kayadelen, H.K.; Ust, Y.: Thermodynamic, environmental and economic performance optimization of simple, regenerative, STIG and RSTIG gas turbine cycles. *Energy* **121**, 751–771 (2017). <https://doi.org/10.1016/j.energy.2017.01.060>
54. Ozsari, I.; Ust, Y.: Effect of varying fuel types on oxy-combustion performance. *Int. J. Energy Res.* (2019). <https://doi.org/10.1002/er.4868>
55. Kayadelen, H.K.: A multi-featured model for estimation of thermodynamic properties, adiabatic flame temperature and equilibrium combustion products of fuels, fuel blends, surrogates and fuel additives. *Energy* **143**, 241–256 (2018). <https://doi.org/10.1016/j.energy.2017.10.106>
56. Demirbas, A.: *Methane Gas Hydrate*. Springer, London (2010)
57. *Gas Composition Transition Agency Report 2013* (2013)
58. Ferguson, C.R.: *Internal combustion engines: applied thermo-science* (1986)
59. Chase, M.W.; Davies, C.A.; Downey, J.R.; Frurip, D.J.; McDonald, R.A.; Syverud, A.N.: In *Janaf thermochemical tables*. Third edition. vol. 14 (1985)
60. Turns, S.R.: *An Introduction to Combustion: Concepts and Applications*. WCB/McGraw-Hill, Boston (2012)
61. Dostal, V.: *A supercritical carbon dioxide cycle for next generation nuclear reactors* (2004)

